SPECTROSCOPIC STUDY OF AN EXPANDED ARGON MICROWAVE (2.45 GHZ) PLASMA AT ATMOSPHERIC PRESSURE IN A HELIUM ENVIRONEMENT

M. C. García,[1] M. Varo and P. Martínez

Departamento de Física Aplicada, Edificio C-2. Campus Universitario de Rabanales. Universidad de Córdoba.

E-14071 Córdoba, Spain, Phone: 34 957212633

[1] *Author for correspondence, e-mail: fa1gamam@uco.es*

ABSTRACT

In the present work, an argon microwave (2.45 GHz) plasma flame created at the end of a surface wave sustained discharge column in helium environment has been experimentally studied. This is a plasma with new possibilities because under some experimental conditions it expands, being less contracted than the plasma flame created in open air. The new expanded discharge could offer additional advantages for applications in which larger extension of plasma were required.

The expansion phenomenon of this plasma flame was studied under different experimental conditions. In every case, the characteristic parameters of this expanded plasma such as electron density, electron and gas temperatures, or density population of excited atomic levels, were measured by using Optical Emission Spectroscopic techniques. From these results, the main advantages of this plasma source were pointed out.

Index Headings: Microwave-induced plasmas, surface-wave-sustained plasmas, plasma flames, plasma spectroscopy.

INTRODUCTION

In the past few years, a significant amount of theoretical and experimental works has been conducted on the behaviour of high frequency (HF) plasmas because their use in a great number of scientific and technological fields has noteworthy grown. Nowadays, these discharges are being employed in elemental analysis,[1-4] surface treatment,[5,6] lighting,[7] destruction of contaminant gases,[8] or sterilization,[9] among other applications.

Surface wave sustained discharges (SWDs) generated in dielectric tubes are a special kind of HF discharges with numerous advantages: they can be generated under a broad range of frequency (over the radio frequency and microwave frequency domains), using different support gases (argon, helium, xenon, nitrogen,…), at different pressure conditions (from few mtorr to several atmospheres), and employing tubes of different shapes (cylindrical or flat) and sizes. These interesting features explain the attention that these discharges have attracted in the last two decades.[10-18]

Among SWDs those generated at 2.45 GHz have been particularly studied. This frequency condition may result interesting in some applications such as Plasma Enhanced Chemical Vapour Deposition for thin film deposition and Plasma Etching, because the use of high frequency plasmas improves the deposition/etching rates.[19,20] SWDs at low pressures provided successful results in applications of this kind.[21-23] But, in the last ten years, the interest in studying SWDs at atmospheric pressure has significantly grown.[24-31] Effectively, this pressure condition simplifies the handling of SWDs, avoiding the use of complicated vacuum systems. Moreover, the atmospheric pressure condition offers additional advantages against the low pressure regime such as higher deposition rates or lower ion bombardment, features that could be very interesting for some applications.

On the other hand, discharges generated using argon as support gas have been widely studied and employed as this gas is relatively cheap and easy to ionize, compared with other inert gases. But, argon SWDs maintained at atmospheric pressure and 2.45 GHz are radially

contracted, not refilling completely the tube that contains them.[32-33] This phenomenon, so called *radial contraction*, is characteristic for DC and HF discharges generated at pressures high enough and, under some experimental conditions, brings associated the *filamentation* effect: the plasma column breaks into two or more filaments of smaller diameters, and it becomes very unstable. In order to avoid it, argon SWDs at 2.45 GHz and atmospheric pressure are usually generated in capillary tubes of radius smaller than 1 mm.

The abovementioned contraction phenomenon is also present in the 2.45 GHz argon plasma *flame* open to the air that can be created at the end of a SWD column, by using a quartz tube short enough.[28,34,35] Both SWD column and flame have been shown to be very stable plasma sources at atmospheric pressure, easy to handle, with a relatively low consumption of microwave power and gas. But their radially reduced sizes limit the possible applications of these argon plasmas, especially in those appliances in that big plasma extensions are required (surface processing, sterilization …). So, it would be interesting to research how to expand them.

In the present work, an argon microwave (2.45 GHz) plasma flame created at the end of a SWD column in helium environment has been experimentally studied. This is a plasma with new possibilities because under some experimental conditions it expands, being less contracted than the plasma flame created in open air.[35] Different expanded flames were obtained by varying the argon and helium gas flow rates. The characteristic parameters of these expanded plasmas such as the electron density and temperature, gas temperature, or density population of excited atomic levels, were measured by using Optical Emission Spectroscopic techniques. From these results, the main advantages of this plasma source were pointed out.

This paper has been organized as follows. The next section briefly describes the experimental arrangement employed to generate and diagnose the discharge. In the subsequent section, the diagnostic techniques employed to determine the fundamental plasma

characteristics are indicated. Two last sections present and discuss the experimental results obtained in this work and finally, draw the most interesting conclusions from them.

EXPERIMENTAL ARRANGEMENT

Plasma generation

Figure 1 shows the experimental set-up used for the creation of the plasma. A *surfaguide* device[10] was used to couple the energy coming from a microwave (2.45 GHz) generator (GMP 12 kT / t SAIREM) to the support gas (argon with a purity of 99.99 %) within a quartz tube of 1.5-4 mm of inner and outer diameter, respectively. In this work the microwave power was set at 240 W level and the length of the tube (2.6 cm from the coupler gap) was adjusted to achieve a plasma flame at its end. The electromagnetic field that sustained the complete discharge (previous column and flame) was provided by a travelling surface wave linked to the plasma-dielectric interface. This surface wave transmitted energy as it propagated throughout the discharge, energy that was partially employed to excite, to ionize and/or to dissociate the different species and molecules existing in the support gas. The radial contraction phenomenon was responsible for the progressive constriction observed at both the end of the plasma column and the subsequent plasma flame.

An external concentric tube (6-8 mm) was employed to allow helium gas (with a purity of 99.99 %) to flow around the discharge tube and the plasma flame. By changing argon and helium flow rates conditions, and the microwave power injected into the discharge, the shape and dimensions of the plasma flame could be modified. In this way, under some particular experimental conditions, an expansion of the plasma flame was observed. In these cases, the flame showed both: i) a more *luminous zone* having radial dimensions of the inner tube and ii) a *diffuse zone* expanding toward the walls of the outer tube (details about the shape and geometry of this plasma flame are shown in Fig. 2). Moreover, when the flame was expanded the contraction in the end part of the plasma column also disappeared.

4

The length of the external tube was set long enough to avoid the contact plasma-air and reduce the air entrance into the plasma flame. This configuration permitted us a better control of the species existing in the plasma, which could be interesting in applications requiring controlled environments.

The expansion phenomenon was studied under different experimental conditions. In this paper, the results of the study of several expanded flames generated by using a given argon flow rate (F_{Ar} = 0.560 slm) and different helium gas flow rates (F_{He} = 0, 0.140, 0.340 and 1 slm) are presented.

Optical measurements

Figure 1 includes a scheme of the optical detection assembly and data acquisition system to process spectroscopic measurements. Light emission from the plasma was analyzed by utilising a Jobin-Yvon Horiba 1000M spectrometer (Czerny-Turner type) with 1 m of focal distance, a holographic diffraction grating of 2400 groves/mm, and a typical spectral dispersion of 0.4 nm/mm in the visible range. The OH and H_β spectra were recorded using a Hamamatsu R928P photomultiplier as detector and slit widths of 50 μm. The emission spectra from 220 to 730 nm were recorded employing a cooled CCD camera (Horiba Jobin Yvon) and slit widths of 100 μm. The light was side-on collected at each axial position of the plasma through an optical fibber (UV-VIS high OH fibber with a range of transmission wavelength 200-800 nm). A UV-VIS collimating beam probe was coupled to the optical fibber giving a 0º-45º of field of view and 3mm of aperture. Thus, an Abel inversion was precluded and the radial study of the plasma could not be performed. Consequently, the values reported for the quantities measured in this work should be considered to be average ones for a transversal section of the plasma associated with a specific axial position. The axial origin of the measurements was located at the beginning of the plasma (y-axis). The flame started at the y =

2.6 cm position (end of the quartz tube). Intensity measurements were calibrated by using a calibrated ribbon lamp with a known emission spectrum.[36]

SPECTROSCOPIC DIAGNOSIS

The *electron density n_e* was determined from the H_β Balmer series line of the hydrogen atomic system (486.13 nm). The hydrogen atoms were present in the discharge as impurities in the carrier gas (argon and helium of 99.99% of purity). The analysis of the Stark broadening of H_β line is one of the most common tools for the diagnostic of the plasma electron density due to its Stark broadening has a small dependence on electron temperature and to slight effect over its profile of phenomena such as ion dynamics.[37] In the present work the Gigosos et *al.*[38] expression was used to calculate n_e from $\Delta\lambda_S$ (H_β) (full width at half-maximum FWHM of the Stark unfolded line)

$$\Delta\lambda_S(H_\beta) = 4.800\,nm \times \left(\frac{n_e}{10^{23}\,m^{-3}}\right)^{0.68116}$$

(1)

with n_e in m^{-3} and the $\Delta\lambda_S$ in nm. The calculations cover the n_e-range of between 10^{20} and 10^{25} m^{-3} and of T_e between 1 000 and 17 500 K.

The magnitude of the experimental Stark broadening of the H_β line was calculated by fitting numerically its experimental profile to a Voigt function (a result of the convolution of a Gaussian function with a Lorentzian function). The Lorentzian part of the profile corresponded to the contribution of the Stark and Van der Waals broadenings. Under the experimental conditions of plasmas studied, the Lorentzian part of the H_β profile could be largely ascribed to the Stark effect.[39] The error in the data, obtained from the standard deviation of n_e upon repeating the H_β recording 6 times at a given plasma position, was 20 %.

The *gas temperature T_{gas}* was considered equal to the rotational temperature T_{rot} obtained of the rovibrational spectrum for the Q_1 branch of (0-0) band of the OH radical

(between 306 and 311 nm), which resulted from the dissociation of water traces present in the plasma gas. At atmospheric pressure, the highly favourable energy exchange between heavy particles in the plasma and the internal roto-vibrational states of these molecular collisions allowed us to make this assumption.[40] Ricard *et al.*[41] from simulations of OH spectra have found the OH band was a reliable thermometer for $T_{gas} \leq 1800$ K. The value of T_{gas} was taken from the slope of the plot of $\log(I\lambda/A_{J'J''})$ as a function of transition upper state energy, I being the maximum value of the line intensity and $A_{J'J''}$ the corresponding transition probability (Table I). The standard deviation on T_{gas} was under 15% upon repeating the recording six times.

The *excitation temperature* was estimated from the slope of the Boltzmann plot (a $\log(n_p/g_p)$ vs. excitation energy plot) for the upper levels (5p and higher) of the argon atomic system. This diagram is a representation of the argon Atomic State Distribution Function (ASDF), and its shape depends on the degree of equilibrium existing in the discharge.[42] In a plasma in Local Thermodynamic Equilibrium (LTE), the Boltzmann plot fits a straight line whose slope is related to excitation temperature. But argon SWDs at atmospheric pressure are not in LTE,[24-28,30,34,35] being these plasmas in a partial Local Saha Equilibrium recombining (pLSE recombining) in which only the levels just below the ion ground state conform the Saha-Boltzmann equilibrium, with the rest of levels lying below the LTE straight line. In plasmas with electron densities high enough the excitation kinetics is controlled by electron collisions and the excitation temperature can be considered as an estimation of the *electron temperature*. So, in the present work the Boltzmann-plot allowed both to estimate electron temperature and find out the type of equilibrium existing in the plasma. The error in the measured values of T_e was found (from the standard deviation upon repeating the recordings six times) not to exceed 15%.

The *absolute population densities n_p* of the different excited levels of the argon atomic system were determined from calibrated intensity measurements I of the spectral lines (peak

area) corresponding to atomic transitions starting at each p specific level, using the following expression:

$$n_p = \frac{4\pi\lambda I}{hcA_{pq}\Lambda_{pq}l}$$
(2)

where A_{pq} is the coefficient for spontaneous emission from level p to level q, λ the wavelength of the corresponding transition, l the flame diameter and Λ_{pq} the escape factor of this transition. Table II shows the atomic lines used in the representation. Measurements of light absorption have revealed that, in the observation direction, the plasma flames studied were optically thin for all studied transitions ($\Lambda_{pq} = 1$). The error in the n_p measurements of about 20 % was mainly determined by the accuracy of the absolute intensity calibration.

RESULTS AND DISCUSSION

Radial and axial expansion of the plasma flame

At a defined microwave power level, for a given value of argon flow rate the shape and dimensions of the plasma flame formed at the end and out of the inner tube varied when the experimental conditions of external helium flux were changed. In this way, under some specific experimental conditions, contraction reduced and a plasma flame refilling the outer external tube was achieved. Moreover, the axial dimensions of the flame also varied with the external flow rate of helium. In this way, for an argon flow rate of 0.560 slm and 240 W of microwave power, when increasing the helium flow rate the flame started to expand (radially and axially) and under high enough helium flow rate conditions the plasma contracted again. For a helium flow rate of about 1 slm the most expanded flame was achieved. It was proved that under other argon flow rate conditions, the helium flow rate that made the expansion maximum was different (to $F_{Ar} = 1$ slm corresponded a $F_{He} = 2$ slm).

8

The change in the thermal conductivity of the main gas, could have limited the effect of the contraction phenomenon in the expanded flames. Effectively, the presence of helium around the flame could provoke a plasma expansion because of the higher thermal conductivity for the helium, which reduced the non-uniform gas heating along the discharge radius, typical of argon microwave (2.45 GHz) plasmas at atmospheric pressure. This fact has been explained by Castaños-Martínez et al.[33] Effectively, a higher thermal conductivity implies a lower radial gradient of T_{gas} which provokes a lower radial gradient of ions towards the wall. This originates a much lower loss of charged particles by recombination at the positions nearest the wall, resulting in a higher plasma radius. Kabouzi et al.[32] and Castaños-Martínez et al.[33] have also explained that the non-uniform radial heating could be also considered responsible for the contraction of pure argon discharges due to its influence on the atom density N, and therefore on the reduced electric field E/N. The ionization rate depends exponentially on E/N, so in argon plasmas because N increases from the axis to the wall, E/N decreases and so does the ionization rate. In a certain radial position the ionization process no longer compensates for the charge particle losses: the end of the plasma established.

When the plasma was refrigerated with argon (instead of helium) the expansion was not observed. This result is consistent with the precedent argument explaining the discharge expansion: now the external gas has the same ionization potential and thermal conductivity, so contraction is again stronger.

Electron density and temperatures

The axial profiles measured for the *electron density* are depicted in Fig. 3. In the non-cooled flame, electron density took the highest values ($6 \cdot 10^{14}$ cm^{-3}), as it was expected because of the radial contraction that it exhibited, having values similar to the corresponding column zone ones ($y = 2.6$ cm position). A sharp decrease of n_e from the $y = 3.5$ cm position was observed indicating the end of the plasma flame.

When increasing helium flow rate, n_e decreased noteworthy, from $4 \cdot 10^{14}$ cm^{-3} in the column zone to $7 \cdot 10^{13}$ cm^{-3} (value that can be considered as an estimation because it is slightly outside the validity range of the Gigosos *et al.* formula) in the flame zone. This result agrees with the fact that in the flame region the discharge expands occupying a larger volume, which results in a lower average electron density characteristic of expanded plasmas. Besides, in this zone, one part of the plasma energy could be employed in the excitation and ionization of the surrounding helium gas, with higher excitation energies and ionization potential, also resulting in a lower electron density.

The electron temperature at each axial position of the different plasma flames was estimated from the slope of the corresponding Boltzmann plot for *5p* and higher levels of the atomic system of argon. Fig. 4 shows the example corresponding to y = 5.6 cm axial position of the plasma flame generated by using F_{Ar} = 1 slm and F_{He} = 1 slm. In this case, it can be observed that the excitation temperature obtained including the *4p* levels in the calculation is slightly lower because these levels are not likely in pLSE.

Figure 5 shows the axial profile of electron temperatures measured for the different flames studied. In the non-cooled flame the electron temperature sharply felt down from about 8000 K to 5200 K at the positions farthest from the coupling device. When cooling with helium, the electron temperature in the previous plasma column is some lower (about 7000 K) decreasing to 4000 K in end part of the flame zone. So, the outer helium flow surrounding the argon flame seems to affect the T_e values, cooling the gas of electrons. On the other hand, the axial profile of T_e showed a smoother gradient in those cases in which axial plasma dimensions were higher.

The axial profiles of T_{gas} measured for the different flames are depicted in Fig. 6. In the non-cooled flame the gas temperature had a constant value of about 1800 K, higher than those measured in the previous SWD column (1300 K). A similar behaviour was observed by García *et al.*[35] when studied a similar argon plasma flame open to the air. When increasing the

external helium flow rate, the gas temperature was progressively decreasing to 1200 K. So, the presence of an outer helium flow also permits to reduce the gas temperature of the discharge, what could result very interesting in case they were used in applications in which low gas temperatures are required (such as surface treatments or depositions).

From these results, it can be deduced that the expanded plasma flame is a typical two-*temperature* (*2T*) discharge (with $T_e \gg T_{gas}$).[42] The big difference in mass between electron and heavy particles is responsible for the inefficient exchange of kinetic energy through collisions among them.

As a resume, it can be concluded that the external helium flow does affect the characteristic parameters of the plasma flame reducing its electron density and temperature and its gas temperature. So, it can be expected that the external cooling with helium affects the microscopic kinetics of this plasma region.

Excited species in the expanded plasma flame

In order to comprehend the excitation kinetics in the expanded plasma, an exhaustive study of the visible spectra emitted by *column* and *flame* plasma regions in the discharges studied was performed.

Atomic helium lines were not detected in either case, which indicated that the excitation of helium atoms in the plasma *flame* was not effective enough to allow the detection of helium lines. This was an expected result (the emission of atomic and ionic helium lines has been neither observed in the spectra emitted by the argon-helium SWD column sustained at atmospheric pressure studied by Muñoz and Calzada[43], even when microwave power at 2000 W level was employed) because of the high excitation energy of the excited (and metastable) helium levels and the high ionization potential of this gas.

The spectra registered in the *plasma column region* showed: 1) a relatively strong emission of lines of the Ar I system, of lines of H I system (H_α, H_β and H_γ) and of the

rotational spectrum of the OH radical (band head at 308.9 nm); 2) and a weak emission of the rotational band of NH (336.0 nm band head), of the rotational band of CN (388.3 nm band head), and of the rotational spectrum of N_2^+ (band head at 391.4 nm).

The spectra emitted by the *expanded plasma flame* mainly showed lines of Ar I and H I systems. Since the plasma expanded to the walls of the external tube, some plasma etching of its inner wall took place, and some new lines corresponding to impurities in the quartz were observed. In this way, two very intense lines appeared in the spectra at 588.9 nm and 589.6 nm, corresponding to Na I system. As far as the rotational bands are concerned, the OH rotational band showed a weak emission but this band was clearly discernible in all cases studied. The NH and N_2 (band heads at 315.9, 337.1, 353.3, 357.7, 375.5, 380.5, 398.8 and 405.9 nm) rotational bands showed very weak emissions but their heads were clearly noticeable in all studied cases. Under conditions of low helium flow rates the emission of the abovementioned bands strongly intensified and new rotational bands were observed (see Fig. 7 (a)): NO (band heads at 237.0, 247.9 and 259.6 nm), CO (band heads at 266.5, 283.3 and 297.7 nm) and N_2^+ (band heads at 356.4, 358.2, 391.4, 419.9, 423.6, 427.8, 465.2 and 470.9 nm). These emission bands were likely related to the air (coming from outside) existing in the outer tube. So, in this plasma flame, a helium flow high enough pushes the air out of the system making the emission of NO, CO and N_2^+ undetectable (see Fig. 7(b)).

In the argon and helium gases used in the present work, molecular gases like CO_2, H_2O and N_2 are present as impurities at trace levels. Timmermans *et al.*[44] have explained that in microwave (2.45 GHz) argon plasmas sustained at atmospheric pressure, excited diatomic association molecules are most likely created by three body association:

$$A + B + S \rightarrow AB^* + S \tag{3}$$

in which the heavy particles A and B associate in the presence of a spectator S. This process could explain the observation of CN and NH bands. Effectively, Timmermans et al.[44] have also explained that a possible creation channel for nitrogen atoms needed for these association reactions could be:

- *Charge transfer* reaction

$$Ar^+ + N_2 (X) \rightarrow Ar + N_2^+ (X) \tag{4}$$
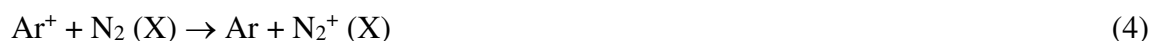
- Followed from the *dissociative recombination* reaction

$$N_2^+ (X) + e^- \rightarrow N + N \tag{5}$$

On the other hand, C atoms come from the dissociation of CO_2 and OH radical arise from the dissociation of water.

Figure 8 depicts the axial behaviour of the absolute population densities n_p of *5p*, *5d* and *6d* argon atomic levels for one of the expanded flames studied (F_{He} = 0.340 slm). It can be observed that the population densities of Ar I excited levels show similar dependency on the experimental conditions to that of the electron density. This occurs for all plasma flames studied, which is consistent with the fact that the excitation kinetics in this discharge region was controlled by electron collisions.

Figure 9 represents the axial distribution of 588.9 nm and 589.6 nm atomic sodium spectral lines observed for the flame generated with an argon flow rate of 0.560 slm and helium flow rate of 0.340 slm. This figure shows the existence of a maximum at a certain position of the plasma flame (near where erosion of inner wall of external tube was higher). The excited lines observed corresponded to transitions from *3p* Na I levels (of very low excitation energy 2.10 eV) to the atomic ground state. In the non-cooled flame these lines were not detected because plasma did not reach the tube wall.

Figure 10 shows the axial behaviour of the intensity of the band head of the OH rotational band for the different flames studied. The presence of 0.140 slm of helium around

13

the argon flame highly enhanced the emission of OH rotational band. At higher helium flow rates this emission decreased, which indicated that the radiation observed mainly corresponded to emission of the outermost radial region of the plasma: again, at helium flow rates high enough the lower residence time disfavours the excitation. A similar behaviour was found for the band head of NH rotational band.

In short, as it was expected, the microscopic kinetics in the plasma flame was affected by the helium cooling. In this way, the excitation of argon atoms varied following the electron density changes provoked by the cooling. On the other hand, the presence of helium favours the formation of OH and NH radicals. Finally, a high enough external helium flux avoided the air entrance into the discharge, lowering the concentration of contaminant species in the discharge, which allows a better control of the processes occurring in it.

CONCLUSIONS

In this work the expansion of an argon flame created at the end of a SWD column generated at atmospheric pressure and frequency of 2.45 GHz has been studied. Creating an appropriate ambience of helium around the flame, it can expand until the walls of an external tube. This new expanded discharge could offer additional advantages for applications in which larger extension of plasma were required.

A spectroscopic study of the plasma flames generated under different experimental conditions was performed and the results obtained were compared. In this work has been proved that the gas temperature of the argon flame can be reduced (from 1800 to 1200 K) by cooling with an external helium flow.

When cooling with helium, the electron temperature in the previous plasma column decreases from 8000 K to 7000 K, and it also lessens in the flame region (up to 4000 K in the end part of the flame zone). So, the outer helium flow surrounding the argon flame affects the T_e values, cooling the gas of electrons.

The electron density values measured (7.0×10^{13} and 1.8×10^{14} cm^{-3}) in the expanded flames were lower than those of the previous column (4-6×10^{14} cm^{-3}) and those of the non cooled flame, showing a tendency to decrease toward the plasma end positions. This behaviour was explained taking into account that in this region the volume was higher and moreover by considering that, in this zone, one part of the plasma energy could be employed in the excitation/ionization of the surrounding helium gas.

In all plasma flames studied, the population densities of Ar I excited levels showed the same dependency on the experimental conditions as the electron density, which is consistent with the fact that the excitation kinetic in this discharge was controlled by electron collisions.

A high emission of two lines corresponding to transitions between excited states of Na I system, was observed at some positions of the expanded flame. The presence of sodium in the plasma flame can be ascribed to the erosion of the inner wall of the external tube (which contains sodium impurities) provoked by its direct contact with the plasma.

The presence of helium also provoked an intensification of the radiation emitted by the OH and NH rotational bands (at certain position of the expanded flame) and avoided the entrance of air (coming from the outside) in the flame.

Finally, the cooling with helium permits to obtain: 1) SWD plasma flames and columns of higher volume at atmospheric pressure, which can result very interesting from an applied point of view; 2) SWD plasma flames of lower electron densities at atmospheric pressure, which can be of interest from a spectroscopic point of view (for example, enabling to study the atomic spectral lines broadening under conditions of low n_e); and 3) non-contracted SWD plasma columns at atmospheric pressure, which can be interesting from the point of view of their modelling.

ACKNOWLEDGEMENTS

REFERENCES

1. J. Hubert, M. Moisan and R. Ricard, Spectrochim. Acta B **33**, 1 (1979).

2. M. Selby, R. Rezaaaiyaan and G.M. Hieftje, Appl. Spectrosc. **41**, 749 (1987).

3. J. Hubert, S. Bordeleau, K.C. Tran, S. Michaud, B. Milette, R. Sing, J. Jalbert, D. Boudreau, M. Moisan and J. Margot, Fresenious J. Anal. Chem. **355**, 494 (1996).

4. M.D. Calzada, M.C. Quintero, A. Gamero, J. Cotrino, J.E.S. Uría and A. Sanz-Medel Talanta **39**, 341 (1992).

5. S. Shelz, C. Campillo and M. Moisan, Diamond and Relat. Mater. **7**, 1675 (1998).

6. S. Ilías, C. Campillo, C.F.M.Borges and M. Moisan, Diamond and Relat. Mater. **9**, 1120 (2000).

7. D. Baeuchemin, J. Hubert and M. Moisan, Appl. Spectrosc. **40**, 379 (1986).

8. Y. Kabouzi, M. Moisan, J.C.Rostaing, C. Trassy, D. Guerin, D. Keroack and Z. Zakrzewski J. Appl. Phys. **93**, 9483 (2003).

9. S. Moreau, M. Moisan, M. Tabrizian, J. Barbeau, J. Pelletier, A. Ricard and L. Yahia *J. Appl. Phys.* **88**, 1166 (2000).

10. C.M. Ferreira and M. Moisan, *Microwave discharges: Fundamentals and Applications*, (NATO ASI Series B, Plenum, New York, 1993), Vol. 302.

11. M. Moisan, C.M. Ferreira, Y. Hajlauoi, D. Henry, J. Hubert, R. Pantel, A. Ricard and Z. Zakrzewski, Revue Phys. Appl. **17**, 707 (1982).

12. M. Chaker, P. Nghiem, E. Bloyet, P. Leprince and J. Marec, J. Phys. Lett. **43**, 71 (1982)

13. C.M. Ferreira, J. Phys. D. **14**, 1811 (1981).

14. I. Zhelyazkov, E. Benova and V. Atanassov, J. Appl. Phys. **59**, 1466 (1986).

15. J. Cotrino, A. Gamero, A. Sola and V. Colomer, J. Phys. D. **21**, 1377 (1988).

16. M. Moisan, J. Hubert and R. Pantel, *Contrib. Plasma Phys.* **30**, 293 (1990).

17. M. Moisan, C.M. Ferreira, J. Hubert, J. Margot and Z. Zakrzewski "*Surface-wave sustained plasmas: toward a better understanding of RF and microwave discharges*", XXII Conference on Phenomena In Ionized Gases, Hoboken, N.J. (1995).

18. H. Nowakowska, Z. Zakrzewski and M. Moisan, J. Phys. D. **23**, 789 (1990).

19. M.R. Wertheimer, M. Moisan, J.E. Klemberg-Sapieha and R. Claude, Pure & Appl. Chem **60**, 815 (1988).

20. M.R. Wertheimer and M. Moisan, J.Vac. Sci. Technol. **3**, 2643 (1985).

21. M. Moisan and M.R. Wertheimer, Surf. Coat. Techn. **59**, 1 (1993).

22. L. Paquin, D. Masson, M.R. Wertheimer and M. Moisan, Can. J. Phys. **63**, 831 (1985).

23. A. Barranco, J. Cotrino, F. Yubero, J.P. Espinós, J. Benítez, C. Clero and A.R. González-Elipe, Thin Solid Films **401**, 150 (2001).

24. M.D. Calzada, M. Moisan, A. Gamero, and A. Sola J. Appl. Phys. **80**, 46 (1996).

25. M.C. García, A. Rodero, A. Sola and A. Gamero, Spectrochim. Acta B **55**, 1733 (2000).

26. M.C. García, A. Rodero, A. Sola and A. Gamero, Spectrochim. Acta B **55**, 1611 (2000).

27. M.C. García, A. Rodero, A. Sola and A. Gamero, Spectrochim. Acta B **57**, 1727 (2002).

28. M.D. Calzada, M. Sáez and M.C. García, J. Appl. Phys. **88**, 34 (2000).

29. J. Margot, Phys. Plasmas **8**, 2525 (2001).

30. A. Sáinz, J. Margot, M.C. García and M.D. Calzada, J. Appl. Phys. **97**, 113305 (2005).

31. Y. Kabouzi, D.B. Graves, E. Castaños-Martínez and M. Moisan, Phys. Rev. E **75**, 016402 (2007).

32. Y. Kabouzi, M.D. Calzada, M. Moisan, K.C. Tran and C. Trassy, J. Appl. Phys. **91**, 1008 (2002).

33. E. Castaños-Martínez, Y. Kabouzi, K. Makasheva and M. Moisan, Phys. Rev. E **70**, 066405 (2004).

34. M.D. Calzada, M.C. García, J.M. Luque and I. Santiago, J. Appl. Phys. **92**, 2269 (2002).

35. M.C. García, C. Yubero, M.D. Calzada and M.P. Martínez-Jiménez, Appl. Spectroscopy **59**, 519 (2005).

36. C. Yubero, M.C. García and M.D. Calzada, Optica Applicata **38**, 353 (2008).

37. M. A. Gigosos and V. Cardeñoso *J. Phys. B* **29**, 4795 (1996).

38. M.A. Gigosos, M.A. González and V. Cardeñoso, Spectrochim. Acta B **58**, 1489 (2003).

39. C. Yubero, M.C. García and M.D. Calzada, J. Phys. Soc. Jap. **74**, 2249 (2005).

40. J.M. Mermet, in *Inductively Coupled Plasma Emission Spectrometry, Part II: Aplications and Fundamentals* (Ed. P.W. J. M. Bowmans, Wiley-Interscience, New York, 1987).

41. A. Ricard, L. St-Onge, H. Malvos, A. Gicquel, J. Hubert, and M. Moisan, J. Phys. III **5**, 1269 (1995).

42. J.A.M. van der Mullen, Phys. Rep.-Rev. Sect of Physics Letters **191**, 109 (1990).

43. J. Muñoz and M.D. Calzada, J.Phys.D: Appl. Phys. **41**, 135203 (2008).

44. E.A.H. Timmermans, J. Jonkers, I.A.J. Thomas, A. Rodero, M.C. Quintero, A. Sola, A. Gamero and J.A.M. van der Mullen, Spectrochim. Acta B **53**, 1553 (1998).

FIGURE CAPTIONS

Figure 1. Block diagram of the experimental setup used.

Figure 2. Details of the plasma column and expanded flame.

Figure 3. Measured electron density as a function of axial position for the different flames studied (F_{Ar} = 0.560 slm).

Figure 4. Boltzmann plot of excited argon atoms corresponding to y = 5.6 cm axial position of the plasma flame generated by using F_{Ar} = 1 slm and F_{He} = 1 slm.

Figure 5. Measured axial profiles of electron temperatures for the different flames studied (F_{Ar} = 0.560 slm).

Figure 6. Measured gas temperature as a function of axial position for the different flames studied (F_{Ar} = 0.560 slm).

Figure 7. Optical Emission Spectra measured for the plasma flames generated by using an argon flow rate of 0.560 slm and helium flow rates of: (a) 0.140 slm and (b) 1 slm.

Figure 8. Absolute population densities of some Ar I levels as a function of axial position in the expanded flame generated by setting F_{Ar} = 0.560 slm and F_{He} = 0.340 slm.

Figure 9. Intensities of 588.9 and 589.6 nm spectral lines of Na I system as a function of axial position in the plasma flame generated by using an argon flow rate of 0.560 slm and helium flow rate of 0.340 slm.

Figure 10. Intensities of the band head of the OH rotational band as a function of axial position for the different flames studied (F_{Ar} = 0.560 slm).
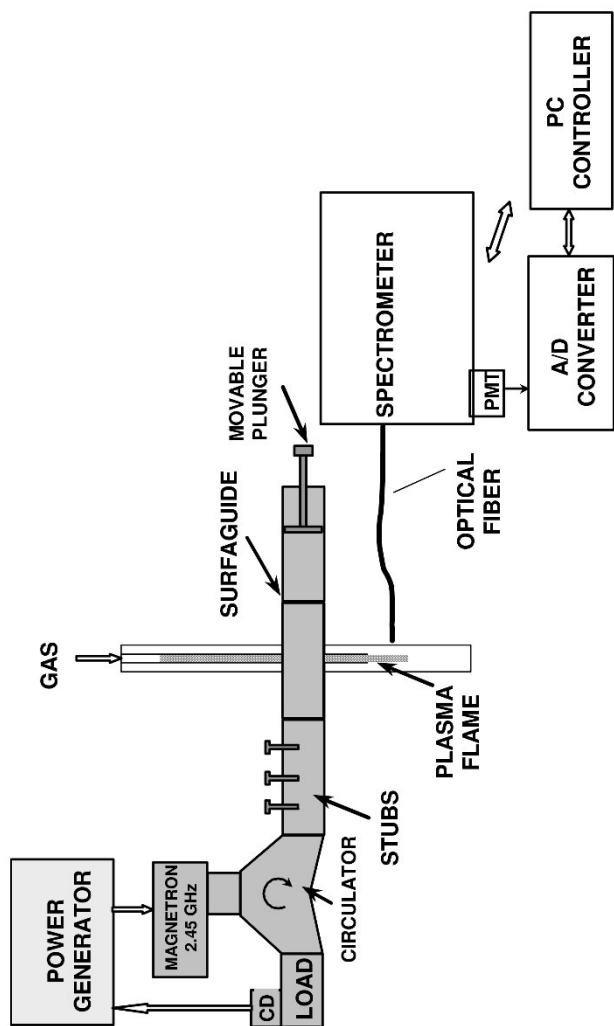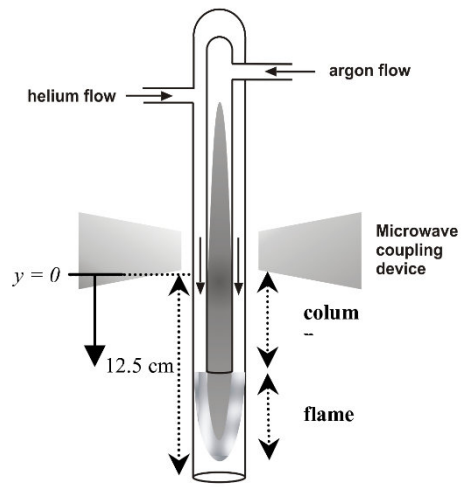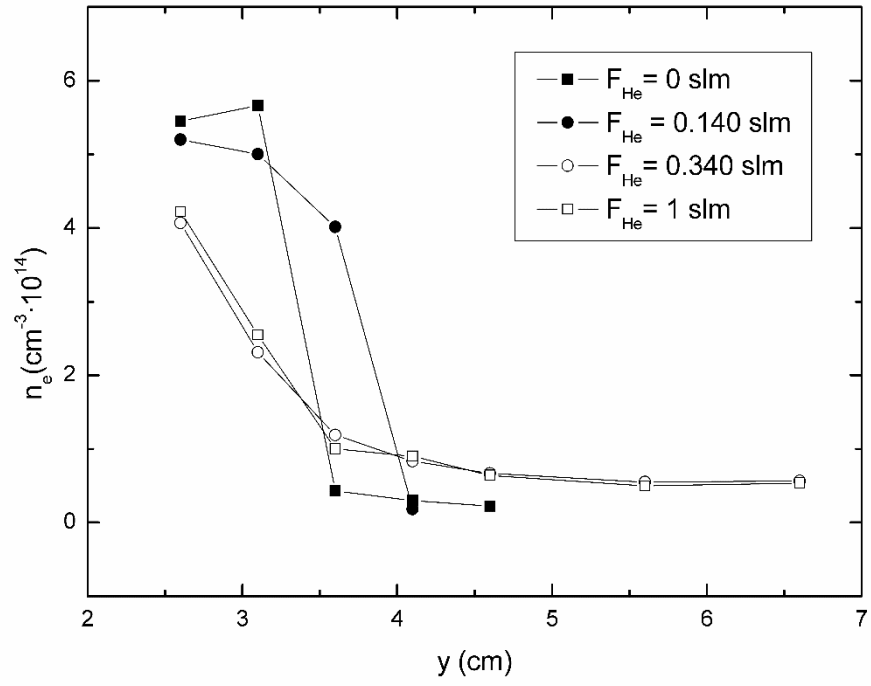
Figure 1

helium flow

argon flow

Microwave
coupling
device

$y = 0$

12.5 cm

colum
--

flame
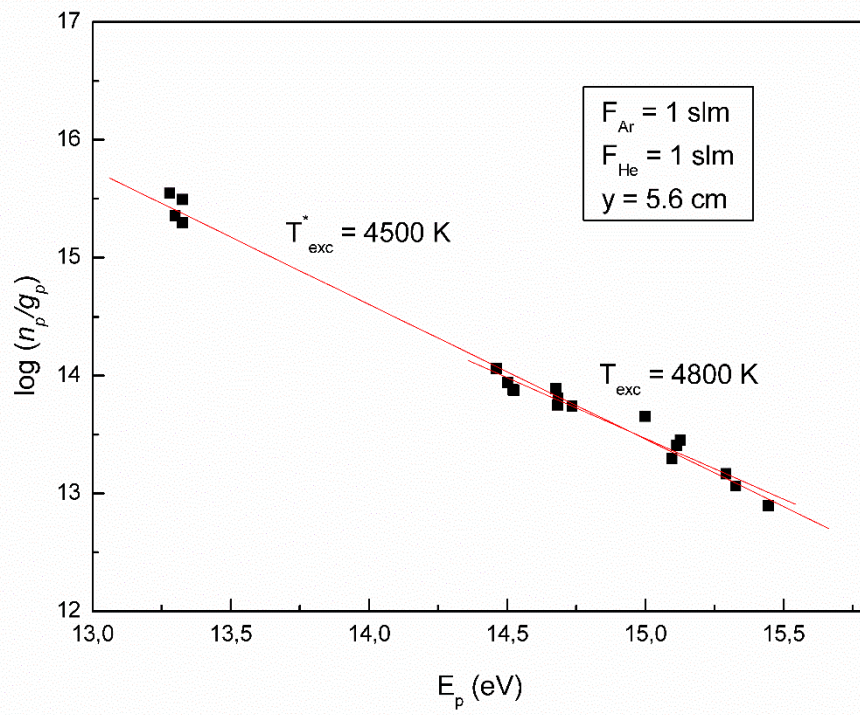
Figure 2

Figure 3

Figure 4
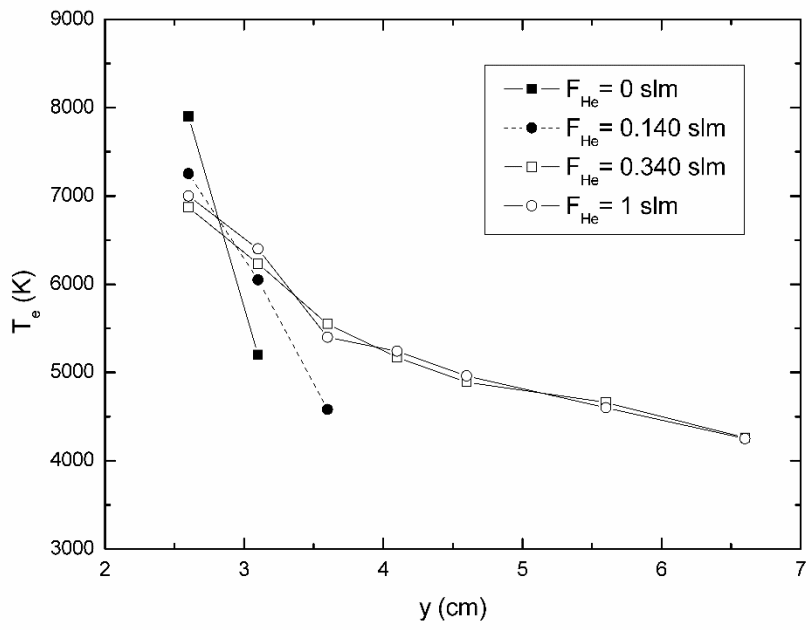
Figure 5
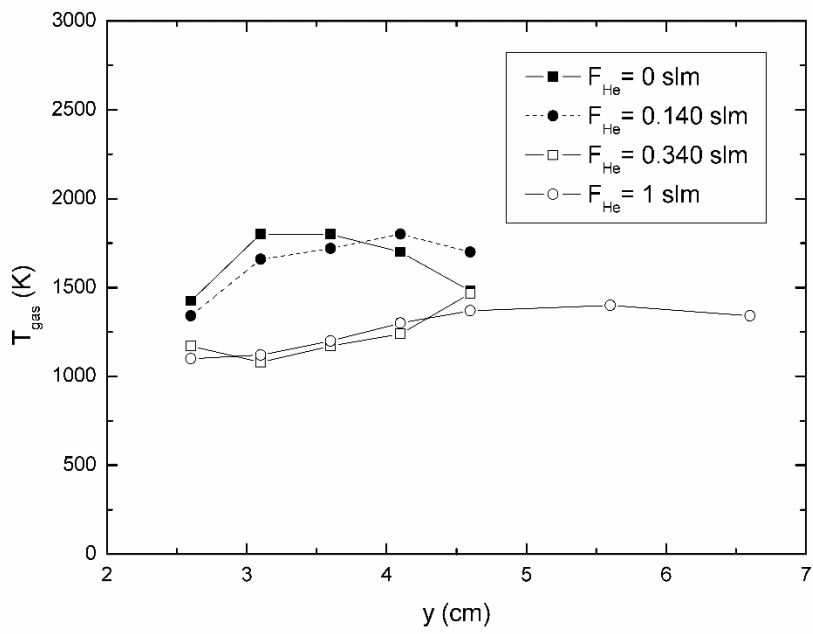
Figure 6
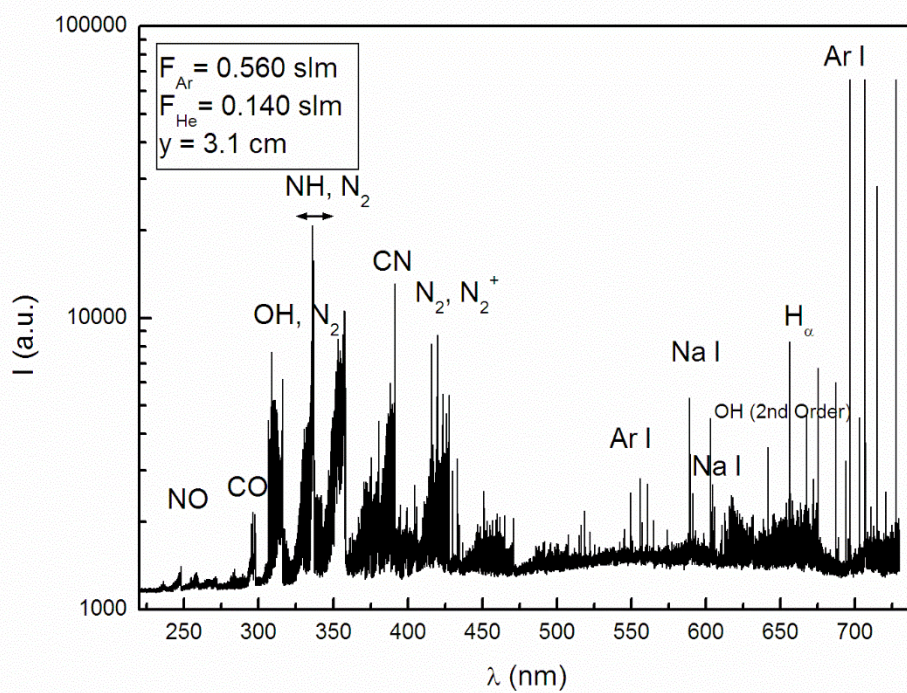
Figure 7a
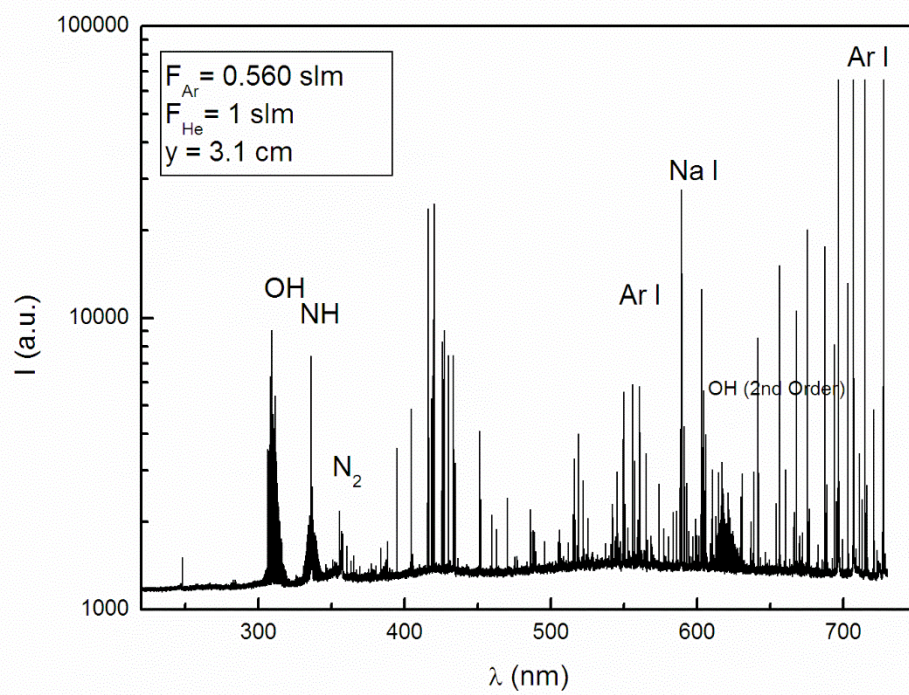
Figure 7b
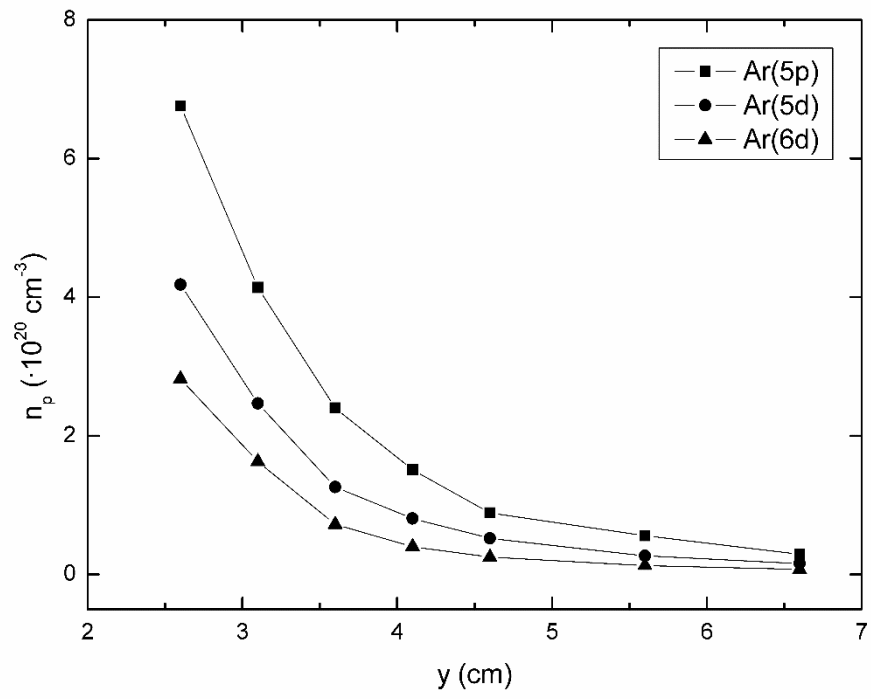
Figure 8
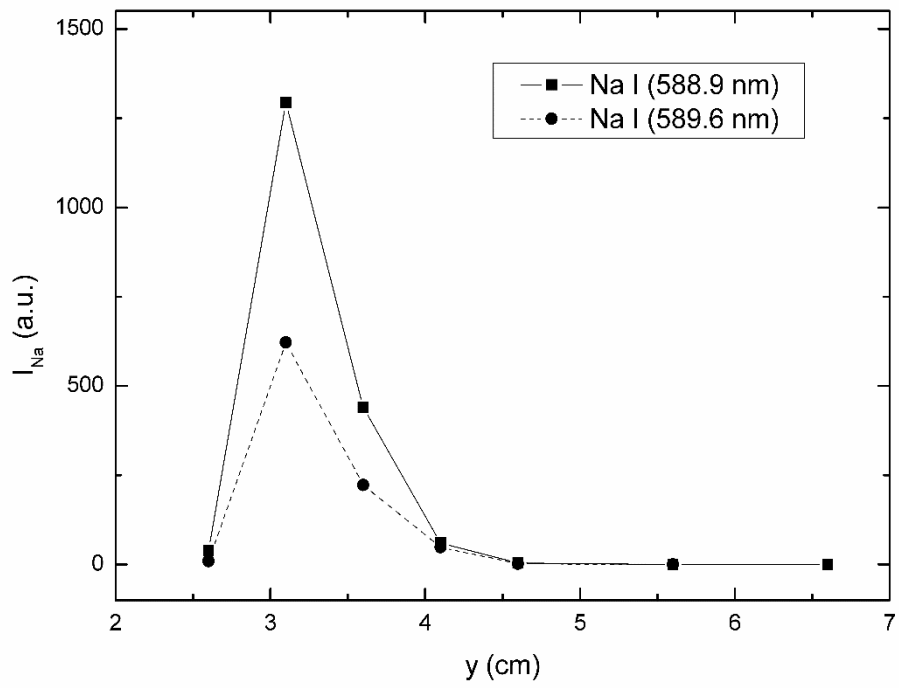
Figure 9
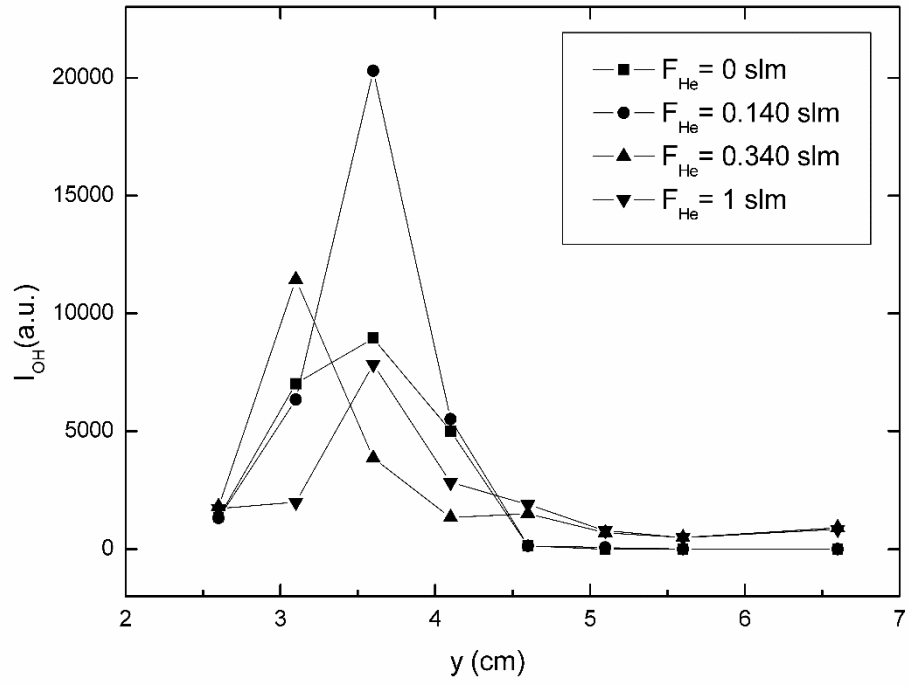
Figure 10

Table I. Characteristic parameters for the Q_1 branch of the OH (0-0) band.

λ (nm)	$A_{J'J''}$ (10^9 s^{-1})	K''	E_p (eV)
307.84	1.00	1	4.0252
307.99	1.70	2	4.0336
308.33	3.37	4	4.0629
308.52	4.42	5	4.0838
308.73	5.06	6	4.1089
309.24	6.75	8	4.1711
309.53	7.58	9	4.2083
309.86	8.41	10	4.2493

Table II. Characteristic parameters of Ar I spectral lines used for excitation temperature determination.

λ (nm)	E_p (eV)	g_p	A_{pq} (10^7 s^{-1})	Transition
714.70	13.2788	3	0.065	4p' - 4s*
706.72	13.2984	5	0.395	4p' - 4s*
727.29	13.3239	3	0.200	4p' - 4s
696.54	13.3239	3	0.67	4p' - 4s*
425.12	14.4598	3	0.013	5p - 4s*
430.01	14.5018	5	0.00394	5p - 4s
427.22	14.5206	3	0.084	5p - 4s
426.63	14.5247	5	0.033	5p - 4s
434.52	14.6763	3	0.0313	5p' - 4s'
433.53	14.6829	3	0.0387	5p' - 4s'
433.36	14.6840	5	0.06	5p' - 4s'
425.93	14.7338	1	0.415	5p'-4s'
675.28	14.7383	5	0.201	4d - 4p
641.63	14.8345	5	0.121	6s - 4p
591.21	14.9992	3	0.0105	4d'- 4p
565.07	15.0961	1	0.333	5d - 4p
560.67	15.1133	3	0.229	5d - 4p
603.21	15.1261	9	0.246	5d – 4p
555.87	15.1324	3	0.148	5d - 4p
518.77	15.2918	5	0.138	5d' - 4p
549.58	15.3265	9	0.176	6d - 4p
522.12	15.4451	9	0.092	7d - 4p